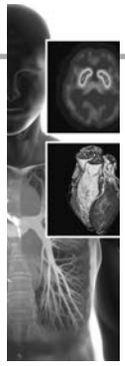

Imaging of short and ultrashort T_2 and T_2^* tissues using clinical MRI systems

There are now a variety of new techniques available to detect signal from tissues with short or ultrashort T_2s and T_2*s. There are also many methods of developing image contrast between tissues and fluids in the short T_2 or T_2* range, which can provide visualization of anatomy that has not previously been seen. Particular methods have been developed to target susceptibility effects, and allow accurate quantitation by compensating for the anatomical distortion produced by these effects. Specific methods have been developed to image the effects of magnetic iron oxide particles with positive contrast and to correct for the loss of signal and image distortion near to metal caused by gross susceptibility effects. These methods are likely to provide interesting options and increase the range of applications of MRI.

KEYWORDS: short T_2 tissue components ■ susceptibility ■ ultrashort echo time

Graeme M Bydder
Department of Radiology, University of California, San Diego, 200 West Arbor Drive, San Diego, CA 92103–8226, USA
Tel.: +1 619 471 0506
Fax: +1 619 471 0503
gbydder@ucsd.edu

During the first year of clinical MRI, only steady state free precession, T_1-weighted and proton density-weighted clinical images were available [1–3]. Heavily T_2-weighted spin echo (SE) sequences arrived suddenly in early 1982 and transformed the practice of magnetic resonance (MR) [4–6]. Images obtained with these sequences detected intermediate or long T_2 relaxation components in tissue. Even with the subsequent development of new classes of sequences, such as fast SE, clinical diffusion-weighted imaging and fluid attenuated inversion recovery, the detection of signal from intermediate and long T_2 relaxation components remains the dominant form of MRI for the diagnosis of parenchymal disease in the brain and much of the rest of the body.

However, even when clinical MRI began, very short mean T_2 relaxation components were recognized in the cortical bone by Smith *et al.* [7] and Edelstein *et al.* [8]. This tissue showed no MR signal. The lack of signal was useful in providing a low-signal background against which abnormalities in cortical bone with sufficiently long mean T_2s to result in detectable signal could be recognized, but the absence of signal from normal cortical bone meant that there was no possibility of measuring normal values of mobile proton density (ρ_m), T_1 or T_2. Nor was it possible to study normal perfusion, and there was no opportunity for active contrast manipulation, little or no distinction between adjacent short T_2 tissues and no means of visualizing normal contrast enhancement. As a result, the study of cortical bone and other MR 'invisible' short T_2 tissues, such as tendons, ligaments and menisci, has been far more limited than that of tissues and organs, such as brain, liver and muscle, where tissue mean T_2s are longer and MR signal from them is readily detectable with conventional clinical sequences. However, even these longer T_2 tissues contain significant proportions (e.g., 5–30%) of invisible or undetectable short T_2 relaxation components when they are imaged with conventional approaches.

To image short or ultrashort T_2 tissues that produce no detectable signal with conventional sequences, indirect methods have been used in which signal is obtained from surrounding or associated longer T_2 tissues. When the low- or zero-signal tissue is surrounded by longer T_2 tissue, signal from this tissue can be used to define the boundaries of the zero-signal tissue. It is also possible to characterize some short T_2 tissues by observing the impact that their difference in susceptibility from that of the surrounding longer T_2 tissues has on the signal obtained from the longer T_2 tissue. For example, some features of trabecular bone can be inferred by the effect this tissue has on the MR signal of adjacent red or yellow bone marrow [9]. A third indirect method is possible when short and long T_2 relaxation components are associated, and undergo magnetization exchange. The effect of saturation of the invisible short T_2 components on this exchange can be observed on the detectable longer T_2 components [10] and, thus, inferences can be made regarding the short T_2 tissue and/or the exchange between the shorter and longer T_2 components.

future medicine part of fsg

An alternative to using conventional sequences to study short T_2 tissues in this way is to employ methods that directly detect signal from them. These usually involve the use of short echo time (TE) or ultrashort TE (UTE) sequences to detect MR signals before they have decayed to zero. There are now a variety of sequences of this type available in the clinical domain.

While T_2 is a property of tissue that reflects dipolar and other nuclear interactions, frequently the effects seen with MRI are described more accurately by the observed T_2 or T_2*. This includes effects such as intravoxel dephasing due to B_0 field inhomogeneity, tissue susceptibility differences and chemical shift. Tissue susceptibility effects reflect the fact that solid tissues, such as bone, are generally more diamagnetic than soft tissues, and that some tissues and fluids may be paramagnetic. The effects of some of these differences can be partly or almost wholly reversed by the use of SE sequences.

In some situations, T_2* effects may dominate and it is useful to recognize several different approaches to imaging short T_2/T_2* components in relation to underlying susceptibility differences:

- The first approach essentially sees the problem as imaging of short or ultrashort T_2 components and the basic approach is to use a short TE or UTE to acquire and encode MR signals before they decay to a low level. This may be appropriate in situations where there are only minor susceptibility differences present.
- The second is susceptibility-weighted imaging, where magnitude and phase data are used to recognize a loss of signal from tissue caused by susceptibility effects. It can be direct and/or indirect (where T_2* become too short to detect) and is qualitative.
- Quantitative susceptibility imaging is the third approach. This technique recognizes the fact that susceptibility differences affect the spatial encoding of MR signals and endeavors to correct this and to calculate values of T_2* that accurately reflect T_2 and susceptibility effects.
- Positive-contrast and white-marker imaging techniques address the specific problem of imaging the effects of magnetic iron oxide particles (MIOPs), which shorten T_2 and produce local disturbances of the magnetic field. The aim is to detect the presence of particles with a positive signal and at least, in part, address the problem of field distortion to achieve credible recognition and quantification of the concentration of MIOPs.
- The fifth group of techniques is targeted at imaging in the presence of metal. Metals can produce very large susceptibility effects with loss of signal due to T_2* effects and gross image distortion. The primary objective in this situation is to deal with the image distortion and restore image integrity to a sufficient degree for the images to be clinically useful.

There is some overlap between these approaches. In some situations it may be appropriate to ignore the effects of susceptibility differences in producing image distortion and regard the problem as one of detecting short T_2 signals, whereas in other situations image distortion due to susceptibility is the primary problem that needs to be addressed. Over the previous year, there has been considerable interest in these approaches with solutions now appearing to some problems that were previously intractable for many years.

Tissue properties

The tissues of the human body can be divided into those that are visible, in the sense that they provide detectable signal with clinical MR systems, and those that are 'invisible' because their mean T_2s or T_2*s are too short to provide a detectable signal. All tissues have multicomponent T_2s. This means that they contain a mixture of short and long T_2 components. The invisible tissues have a majority of short T_2 components and a minority of long T_2 components. The latter components typically do not provide enough signal to be detectable in comparison to image noise levels. The invisible tissues of the body, such as the brain, liver and muscle, have a majority of long T_2 components, which produce the signals seen with conventional techniques. They also have a minority of short T_2 components that do not contribute significantly to the detectable signal.

There is no agreement as to what constitutes a short TE and what is an UTE, and there is an argument regarding how TE should be measured for tissues with short T_2s [11], but for simplicity, a short TE is taken to be less than 10 ms and a UTE less than 1 ms. It is also possible to define short T_2/T_2* as less than 10 ms and ultrashort as less than 1 ms. This reflects the fact that with older systems and SE sequences,

tissues with a T_2 or T_2* less than 10 ms produced little or no signal and were invisible. With more recent systems and gradient-echo sequences the cut-off is closer to 1 ms.

Within the invisible group of tissues (mean T_2 < 10 ms) it is possible to differentiate a first group, including tendons, ligaments and menisci, with short mean T_2s of approximately 1–10 ms, a second group, including cortical bone and dentine, with ultrashort mean T_2s of 0.1–1 ms. There is also a third group, including dental enamel, protons in membranes, large molecules and crystalline bone, with a mean T_2s of less than 0.1 ms.

An important factor in this context is the magic-angle effect [12,13] since it can greatly increase the T_2 of short T_2 tissues, such as tendons, ligaments and menisci. When the orientation of tissues that contain highly ordered collagen is changed, their T_2 varies from a minimum at $\theta = 0°$, where dipolar interactions are greatest, to a maximum where $3\cos^2\theta - 1 \approx 0$ and $\theta = 55°$. θ is the orientation of the fibers to B_0. The increase can be large, for example, from 0.6 to 21 ms [12] or from 7 to 23 ms [13] in the Achilles tendon.

A recently described phenomenon is directional susceptibility in tendons, whereby their bulk magnetic susceptibility varies with orientation to B_0, with signals at the water end of the proton spectrum when fibers are parallel to B_0 and at the fat end of the spectrum (lower frequency) when fibers are perpendicular to B_0 [14]. The difference is relatively large (of the order of three parts per million [ppm]).

The ρ_m of tissues also varies markedly, with bone having a ρ_m of 15–20% and semi-solid tissues, such as tendons and ligaments, having values of 60–70%. ρ_m is generally a more important factor in generating contrast with short T_2 tissues than it is with longer T_2 tissues. The low ρ_m for bone places a limit on the maximum signal that can be obtained from it.

The mean T_1s of some tissues with a majority of short T_2 components are short, with cortical bone having a particularly short T_1, in fact, less than that of fat [15]. The relative differences in mean T_2 or T_2* between normal and abnormal tissue are generally much greater than those in mean T_1.

Relative to air, soft tissues generally show a susceptibility difference of approximately -9 ppm, and bone and calcified tissue of approximately -11 ppm. By comparison, the principal peak of fat resonates at approximately -12 ppm. Paramagnetic materials may show small positive chemical shifts and superparamagnetic materials show greater positive shifts again. Metals including, for example, titanium and some types of stainless steel, may show large positive shifts of 10–100s ppm (or more). These changes in field may be considerably greater than those used by applied machine gradients to encode MR signals and may therefore cause image distortions.

Acquisition methods for short T_2/T_2* components of tissue

Some of the techniques currently being used to detect signal directly from tissues on clinical systems have been used in material science and tissue studies using small-bore high-field spectrometers for many years. Methods now in use on clinical systems are summarized in Table 1. The prototype sequence for imaging short T_2 tissues is single-point imaging where a single point in k-space is acquired with an UTE. This is typically used with 3D phase encoding, which unfortunately makes the technique very time consuming [16].

It is possible to acquire several points at a time, which makes the sequences more time efficient but results in longer TEs for the additional points [17]. There are also free induction decay-based techniques where a radial line of k-space is acquired from the center out [18]. This can be coupled with long T_2 water- and fat-suppression to selectively image short T_2 components [19]. Other trajectories in k-space are possible, including a stack of spirals [20].

Table 1. Short and ultrashort echo time imaging techniques.

Technique	Radiofrequency pulses and gradient	k-space trajectory	Ref.
Single point	Nonselective hard pulse with gradient applied	3D point by point	[16]
Multipoint	Hard pulse with gradient applied	3D partial lines, several points	[17]
Ultrashort echo time	2D two half pulses 3D hard pulse no gradient applied during radiofrequency	Radial, from center out FID acquisition	[18]
Water- and fat-suppressed proton projection MRI	3D hard pulse with gradient on preparation pulses with water and fat suppression	Radial, from center out FID acquisition	[19]
Gradient echo	2D, 3D	Radial rephasing gradients	
Cones, spiral, stack of spirals	3D	Spiral, from center out FID data collection	[20,57]
SWIFT, SEA	3D radiofrequency subpulses	Radial, from center out	[21–24]

FID: Free induction decay; SEA: Simultaneous excitation and acquisition; SWIFT: Sweep imaging with Fourier transform.

A particularly innovative method of imaging short T_2 components is to divide the excitation pulse into subpulses and acquire data after each of these pulses. The acquired data need to be deconvolved with the excitation pulse, but the end result is a much more time efficient acquisition than with typical 3D acquisitions [21–24]. Other techniques that have only been used in the preclinical phase include methods in which radiofrequency absorption, rather than signal detection, is assessed [25]. The methods borrow from older forms of spectroscopy and electron spin resonance, where electronic T_2s are extremely short and may be of the order of a microsecond.

Magnetization preparation, contrast mechanisms & signal-suppression techniques

Traditional contrast mechanisms exploiting differences in ρ_m, chemical shift and other tissue properties can be used in ways that are well known from conventional imaging.

There are also numerous new contrast mechanisms, or old contrast mechanisms operating in new ways, that are of interest in imaging short/ultrashort T_2/T_2* components in tissue. Some of these are listed in Table 2. They are typically used in conjunction with the acquisition techniques detailed in the previous section. These provide a wide range of possible ways of effecting magnetization. For example, 90 and 180°, fat saturation and magnetization transfer pulses can all be used to suppress unwanted long T_2 signals and to produce T_2 contrast in the short T_2 range. There are also relatively new potential mechanisms involving double quantum filters [26] and a reduction in dipolar coupling [27,28]. These techniques are usually applied in conjunction with one of the acquisition methods described in the previous section.

Susceptibility-weighted imaging

Susceptibility-weighted imaging has been in use for a considerable time. It usually exploits reductions in T_2* to develop contrast, and imaging may utilize both magnitude and phase data [29,30]. The T_2* may be so short that this, in effect, becomes an indirect form of imaging utilizing the reduction in signal of adjacent longer T_2 components. The applicability of the technique and related methods can be expanded by utilizing forms of data collection with TEs or UTEs that can detect signal from very short T_2* components [31].

Quantitative susceptibility imaging

Quantitative methods of imaging susceptibility changes need to account for errors in spatial encoding, which may require solutions to a complex inverse problem [32,33]. To date, it has mainly been applied to brain imaging.

Positive-contrast & white-marker imaging

These forms of imaging have been used to describe the particular situation with MIOPs that may not only reduce T_2 and T_2*, but also

Table 2. Magnetization preparations, contrast mechanisms and signal-suppression techniques.

Mechanism	Effect	Ref.
90° pulse	Selective excitation of short T_2/T_2* components with or without subsequent long T_2 signal suppression	
180° pulse	Selective excitation of short T_2/T_2* components and inversion of long T_2 components	
180° pulse and nulling	Selective inversion of long T_2/T_2* components with nulling	
Off-resonance saturation	Selective reduction of short T_2 components	[58]
Magnetization transfer	Selective reduction of short T_2 components with magnetization transfer to detectable T_2 components	[59]
Fat saturation	Selective reduction of fat and short T_2/T_2* water signals	
Later image subtraction from first image	Selective reduction of long T_2/T_2* components	
Susceptibility and spectral mapping ultrashort echo time spectroscopic imaging	Direct mapping of field change and susceptibility differences	[31]
Double quantum filter	Selective imaging of protons with strong dipolar coupling	[26]
Dipolar imaging	Comparison of spin echo and magic sandwich echo imaging	[27]
$T_2\rho$ imaging	T_2 in rotating frame	
Gd contrast agents	Detectable short T_2/T_2* in tissues	[60]
Magnetic iron oxide particles	Reduction in detectable signal in short T_2 tissues	[61]
High velocity flow	Phase-shift due to flow can be specifically targeted	[62]

Gd: Gadolinium.

produce local field distortions. A variety of different methods are available. It is possible to selectively excite only off-resonance spins. It is also possible to apply an additional gradient so that only the magnetization of spins in regions affected by MIOPs are refocused. The inhomogeneities from the particles induce echo shifts and these can be used to calculate and correct for the field distortion. The images reflect both tissue MIOP concentration and deviations of the local magnetic field produced by the particles [34–38].

Imaging in the presence of metal

When forms of metal are implanted in the body an extreme situation may arise in which there is very marked T_2* shortening, but the image distortion is so great that images of regions adjacent to the metal are uninterpretable. This has been a longstanding problem. In the past, a variety of solutions have been proposed, but these have had relatively little clinical impact. The recent development of multiacquisition variable-resonance image combination (MAVRIC) [39] and slice encoding for metal artifact correction (SEMAC) [40] has resulted in a remarkable degree of restoration of images that are grossly degraded by a metallic artifact when imaged using conventional approaches. With MAVRIC, irradiation at a range of different off-resonance frequencies is used to detect signals whose resonant frequency has been shifted by metal. With SEMAC, phase encoding is used during slice selection to reallocate signals that are improperly located by the slice selection process. View angle tilting is also used with this technique to correct for errors with in-plane spatial encoding [41].

Imaging of boundaries involving short T_2/T_2* tissues

Structures of interest in the short T_2 range include thin layers such as those in entheses, periosteum and the deep layers of articular cartilage where there are short T_2 tissues, susceptibility effects between the soft (or semi-solid) tissues and bone, as well as partial volume effects between these tissues over curved surfaces. In this situation, high-resolution 3D-isotropic UTE imaging often has a distinct advantage since it can detect short T_2/T_2* signals as well as reduce the impact of susceptibility differences and partial volume effects. Imaging of ordered fibrous structures, such as tendons and ligaments, include some of the previously discussed issues but, in addition, a loss of contrast of the fiber structure or a blurred appearance may arise from obliquity of the fibers relative to the imaging slice. This Filler effect may simulate changes due to disease. There are also distinctive artifacts at boundaries from chemical shift effects, including those associated with radial acquisitions.

Clinical applications

There are now 2D and 3D UTE sequences available with imaging times of 5–6 min and clinically acceptable spatial resolution. In general the difficulty of acquiring short/ultrashort T_2/T_2* signals means that invisible tissues are imaged at lower spatial resolutions, but with signal levels and contrast that are not attainable with conventional techniques. A balance is necessary to obtain novel qualitative and/or quantitative information at spatial resolutions that show anatomical features with acceptable clarity.

■ Cortical bone

Cortical bone can be imaged with high signal [15]. The T_2 is approximately 0.4 ms and T_1 250–350 ms at 1.5 T, which is shorter than typical values for fat. The mobile proton density is approximately 15–20%. These data can be used both for quantitative [42] and qualitative studies (Figure 1).

■ Tendons, ligaments & entheses

In conventional sequences, the signal from tendons, ligaments and entheses is very low or zero. Entheses are the attachment sites of tendons, ligaments and capsules to bone. They typically contain calcified and uncalcified fibrocartilage (which both have short T_2s). These tissues have a major role in dispersing mechanical stress at the junction between flexible tendons or ligaments and rigid bone.

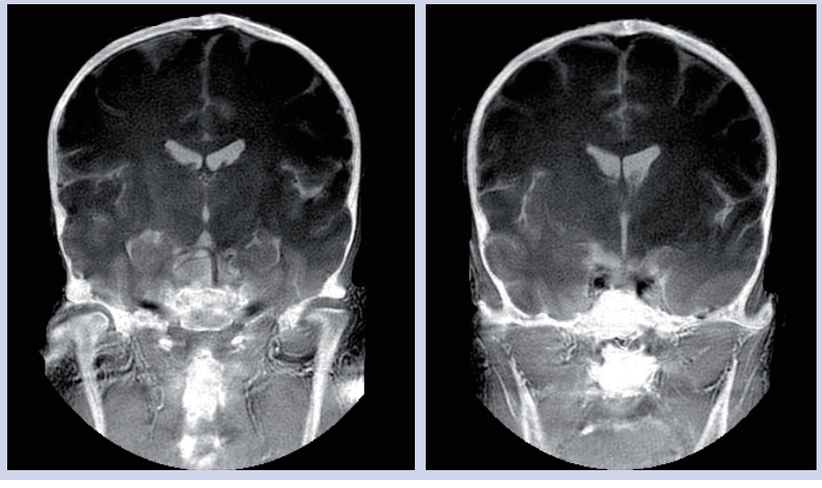

Figure 1. Ultrashort echo time MRI of the skull. The inner and outer tables of the skull are seen in a manner similar to x-ray CT with bone windows.

Tendons and ligaments contain endotenon and endoligament, which have longer T_2s than the fibrous components (although they are still in the short T_2 range) and less magic-angle effect. Uncalcified fibrocartilage has a longer T_2 than the tensile components of tendons as well as an increase in T_2 caused by the magic-angle effect, but this may be present over a wider range of angles reflecting the more dispersed arrangement of the fibers within it. Magic-angle effects may result in a longer T_2 adjacent to bone from fibers that change in direction, from parallel to the bone surface to perpendicular to it, as they insert into bone. Tendons and ligaments can readily be seen with UTE sequences and entheses have been studied in detail [43,44]. Off-resonance fat-suppression pulses reduce the signal from short T_2 fibers (which have a broad line width) more than endotenon or enthesis fibrocartilage (which have longer T_2s and narrower line widths) and this can be an effective contrast mechanism. Inversion pulses may be used to selectively invert and null enthesis fibrocartilage (exploiting its longer T_2), and so, visualize this tissue with high contrast. It is also possible to visualize oblique and transverse fibers in tendons using a combination of fat-suppressed UTE sequences to reduce short T_2 tissue water components and magic-angle imaging to lengthen the T_2 of the fibers at particular angles to B_0 (Figure 2).

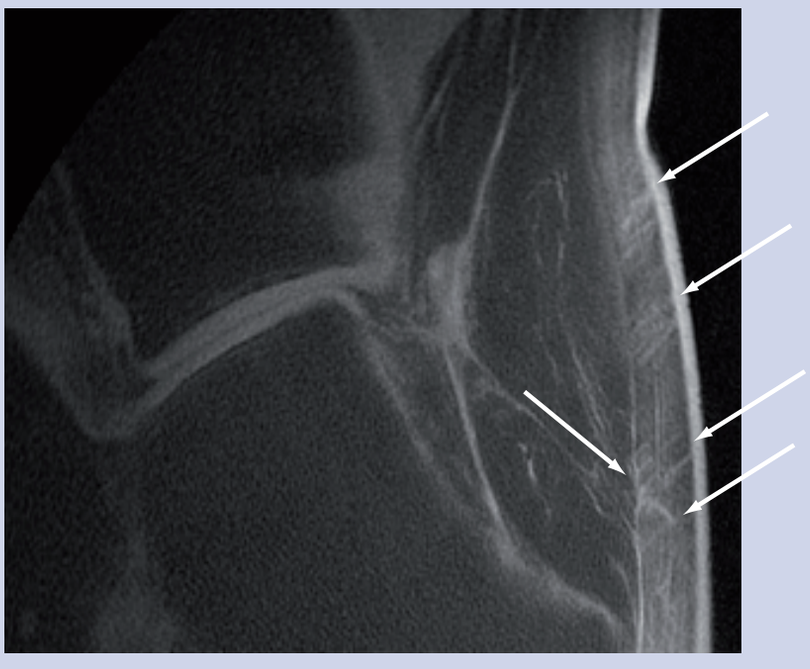

Figure 2. Ultrashort echo time image of the Achilles tendon. Abnormal oblique fibers are seen within the tendon (arrows).

Entheses are selectively involved in the seronegative spondyloarthropathies, such as ankylosing spondylitis and psoriatic arthropathy. The differential diagnosis is of a loss or reduction in fascicular pattern and includes normal sesamoid fibrocartilage, partial volume effects with a loss of fascicular pattern due to the Filler effect, magic-angle effects and disease.

■ Meniscii of the knee

The central region of the adult meniscus has no blood supply (the white zone) while the more peripheral region (the red zone) has a blood supply. Healing of tears in the white zone is generally unsatisfactory and the preferred surgical strategy is usually resection of the torn tissue. Suture and repair is more successful in the red zone. Distinction between the two zones has not previously been possible with MRI using conventional sequences, despite repeated attempts [45]. However, using UTE sequence and gadolinium-based contrast enhancement, the two zones can be distinguished [46] and provide a basis for surgical planning.

Anatomical descriptions of the meniscus include circumferential, radial, lamella, vertical and meshwork fiber groups. With conventional imaging, some radial fibers may be distinguishable from the majority of circumferential fibers, but with UTE and magic-angle imaging each of these fiber groups can be identified (Figure 3). It is also possible to distinguish the internal structure of the meniscus from that of the root ligaments, and the more central cartilaginous region from the more fibrous peripheral region of the meniscus.

The fiber structure provides a basis for understanding the biomechanics of the knee and the various patterns of tear in the meniscus. It also helps in distinguishing magic-angle effects within fiber groups from degenerative changes.

■ Temporomandibular joint disc

This demonstrated some of the characteristics of the meniscus of the knee. Fiber structure can be seen. Lamella, circumferential antero–posterior and superior–inferior fibers are identifiable.

■ Articular cartilage

Articular cartilage has a range of T_2s from approximately 1 to 30–40 ms from deep to superficial. With conventional imaging, the deep radial and calcified layers as well as the adjacent subchondrial bone are invisible. With UTE imaging, signal is detectable from the deeper layers of cartilage, allowing more superficial cartilage and

subchondral bone to be distinguished [47]. This provides a basis for study of the junction between cartilage and bone, which may be of importance in the pathogenesis of osteoarthritis. Complex magic-angle effects are seen, owing to the fibrous architecture of articular cartilage.

In disease there may be both a loss of signal from the deep layer and an increased extent of the short T_2 associated with deep layers. There is electron microscope evidence of thinning of the deep layers in osteoarthritis but preservation in osteomalacia.

■ Spine

Imaging of the spine includes many visible tissues, therefore, to date, attention has focused on invisible structures such as entheses, the end plate of the disc, and short T_2 components in the intervertebral discs and red bone marrow. Fibrocartilage has also been demonstrated in the functional entheses of the transverse ligament of the atlas and the alar ligament. The dorsal capsule of the facet joints of the lumbar spine are also subject to cartilaginous metaplasia. Evidence of iron deposition can be seen in intervertebral discs in thalassemia [48].

■ Brain

There are significant short T_2 components in many tissues of the body with longer mean T_2s, including the brain, liver and muscle. These components can be specifically detected using UTE and other acquisition methods coupled with techniques that suppress long T_2 signals [49,50].

■ Liver

The liver contains a relatively high proportion of short T_2 components. The T_2*s of these may be prolonged in fibrosis [51]. The fibrosis in this situation is often of a relatively open structure and includes free water.

■ Pelvis

Ultrashort echo time sequences have been applied to study the effects of cryosurgery in carcinoma of the prostate [52]. Freezing of tissues results in a substantial reduction in T_2*.

Quantitative approaches

Quantitation may include specific MR properties, including, in particular, T_2 and T_2* [53,54], the properties of the remaining signal after long T_2 components are suppressed and the ratio of short T_2 to long T_2 components. There are also other features, such as the magic-angle effect and dipolar contrast, which can be characterized.

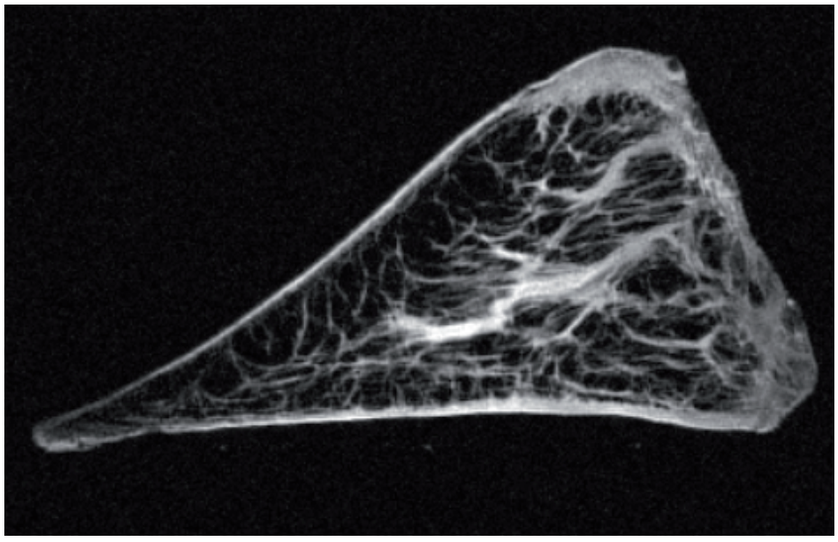

Figure 3. Short echo time image of the meniscus. The lamellar layer, radial and vertical fibers are seen. Circumferential fibers are of low intensity.

There are issues with measuring T_2 and T_2* in the correct range, characterizing different T_2 components (e.g., long and short) including their relative proportions and dealing with artifacts from various sources. Quantitation may be confounded by slice selection and eddy current problems, and by contamination of short T_2 components with long T_2 components that are present in higher concentration.

Future perspective

Imaging of short T_2 and T_2* components is a rapidly expanding area that has seen a convergence of methods targeted at tissues with short T_2 components, susceptibility effects, MIOP imaging and metal artifact control. The methods have improved on solid state imaging, spectroscopy (including continuous-wave methods), electron spin resonance and MR microscopy. The much lower technical performance of clinical systems compared with small-bore spectrometers is a major limitation, but innovative methods for overcoming this problem are now being developed.

The tissues of interest have mainly been in the musculoskeletal system but all tissues of the body have some short T_2 components and study of these may prove to be of diagnostic interest. Some techniques, such as imaging in the presence of metal, are likely to be useful in the clinical domain immediately, while others may require validation and comparative assessment to establish their role. Sodium and phosphorous studies may also be of interest [55,56]. Quantitative approaches may be particularly useful given the large fractional changes in T_2

and T_2* that are frequently seen in disease. The techniques used for imaging often require high gradient performance with control of short-term eddy currents to a level not previously necessary in clinical MR systems. Despite these and other technical difficulties, application to the study of short T_2 and T_2* tissues appears likely to be an area of MRI of considerable importance in the near future.

Financial & competing interests disclosure

The author has received support from General Electric Healthcare. The author has no other relevant affiliations or financial involvement with any organization or entity with a financial interest in or financial conflict with the subject matter or materials discussed in the manuscript apart from those disclosed.

No writing assistance was utilized in the production of this manuscript.

Executive summary

- New forms of data acquisition allow direct imaging of short mean T_2 and/or T_2* tissues.
- Imaging of the short T_2 components in visible tissues may be important.
- New contrast mechanisms provide ways of visualizing previously invisible structures.
- The most significant areas of application have been the musculoskeletal system.
- New techniques for imaging the effects of susceptibility and quantifying these effects are likely to be important.
- Imaging in close proximity to metal is now possible.
- New options for the use of gadolinium chelates and magnetic iron oxide particles are now available.

Bibliography

Papers of special note have been highlighted as:
- ▪ of interest
- ▪▪ of considerable interest

1 Hawkes RC, Holland GN, Moore WS, Worthington BS: Nuclear magnetic resonance (NMR) tomography of the brain: a preliminary clinical assessment with demonstration of pathology. *J. Comput. Assist. Tomogr.* 4, 577–586 (1980).

2 Smith FW, Mallard JR, Hutchison JM *et al.*: Clinical application of nuclear magnetic resonance. *Lancet* 1(8211), 78–79 (1981).

3 Young IR, Hall AS, Pallis CA, Legg NJ, Bydder GM, Steiner RE: Nuclear magnetic resonance imaging of the brain in multiple sclerosis. *Lancet* 2(8255) 1063–1066 (1981).

4 Bailes DR, Young IR, Thomas DJ, Straughan K, Bydder GM, Steiner RE: NMR imaging of the brain using spin-echo sequences. *Clin. Radiol.* 33(4), 395–414 (1932).

5 Bydder GM, Steiner RE, Young IR *et al.*: Clinical NMR imaging of the brain: 140 cases. *AJR Am. J. Roentgenol.* 139(2), 215–236 (1982).

6 Crooks LE, Mills CM, Davis PL *et al.*: Visualization of cerebral and vascular abnormalities by NMR imaging. The effects of imaging parameters on contrast. *Radiology* 144(4), 843–852 (1982).

7 Smith FW: Clinical application of NMR tomographic imaging. In: *NMR Imaging.* Witcofski RL, Karstaedt N, Partain CL (Eds). Bowman Gray School of Medicine, NC, USA 125–132 (1982).

8 Edelstein WA, Bottomley PA, Hart HR *et al.*: NMR imaging at 5.1 MHz: work in progress. In: *NMR Imaging.* Witcofski RL, Karstaedt N, Partian CL (Eds). Bowman Gray School of Medicine, NC, USA 139–145 (1982).

9 Wehrli FW, Song HK, Saha PK, Wright AC: Quantitative MRI for the assessment of bone structure and function. *NMR Biomed.* 19, 731–764 (2006).

10 Henkelman RM, Stanisz GJ, Graham SJ: Magnetization transfer in MRI: a review. *NMR Biomed.* 14, 57–64 (2001).

11 Robson MD, Gatehouse PD, Young IR, Bydder GM: Ultrashort TE (UTE) imaging of short T_2 relaxation components: how should the T_2 weighting be described? *Proc. Intl Soc. Mag. Reson. Med.* 11, 636 (2004).

12 Fullerton GD, Cameron IL, Ord VA: Orientation of tendons in the magnetic field and its effect on T_2 relaxation times. *Radiology* 155(2), 433–435 (1985).

13 Henkelman RM, Stanisz GJ, Kim JK *et al.*: Anisotropy of NMR properties of tissue. *Magn. Reson. Med.* 32, 592–602 (1994).

14 Krasnosselskaia LV, Fullerton GD, Dodd SJ, Cameron IL: Water in tendon: orientational analysis of the free induction decay. *Magn. Reson. Med.* 54(2), 280–288 (2005).

▪▪ **Description of orientation-dependent bulk magnetic susceptibility change in tendons.**

15 Reichert ILH, Robson MD, Gatehouse PD *et al.*: Magnetic resonance imaging of cortical bone with ultrashort TE pulse sequences. *Magn. Reson. Imaging* 23(5), 611–618 (2005).

16 Chen Q, Halse M, Balcom BJ: Centric scan SPRITE for spin density imaging of short relaxation time porous materials. *Magn. Reson. Imaging* 23(2), 263–266 (2005).

17 Fernandez-Seara MA, Wehrli SL, Wehrli FW: Multipoint mapping for imaging of semi-solid materials. *J. Magn. Reson.* 160(2), 144–150 (2003).

18 Bergin CJ, Pauly JM, Macovski A: Lung parenchyma: projection reconstruction MR imaging. *Radiology* 179(3), 771–781 (1991).

19 Wu Y, Ackerman JL, Chesler DA, Graham L, Wang Y, Glimcher MJ: Density of organic matrix of native mineralized bone measured by water-and-fat suppressed proton projection MRI. *Magn. Reson. Med.* 50(1), 59–68 (2003).

20 Qian Y, Boada FE: Acquisition-weighted stack of spirals for fast high-resolution three-dimensional ultra-short echo time MR imaging. *Magn. Reson. Med.* 60(1), 135–145 (2008).

21 Idiyatullin D, Corum C, Park JY, Garwood M: Fast and quiet MRI using a swept radiofrequency. *J. Magn. Reson.* 181(2), 342–349 (2006).

22 Idiyatullin D, Corum C, Moeller S, Garwood M: Gapped pulses for frequency-swept MRI. *J. Magn. Reson* 193(2), 267–273 (2008).

▪▪ **Description of advanced method of acquisition and data collection.**

23 Weiger M, Pruessmann KP, Hennel F: Reconstruction strategies for MRI with simultaneous excitation and acquisition. Presented at: *International Society for Magnetic Resonance in Medicine 17th Scientific Meeting and Exhibition*. Honolulu, HI, USA, 18–24 April 2009.

24 Blümlich B, Gong Q, Byrne E, Greferath M: NMR with excitation modulated by Frank sequences. *J. Magn. Reson.* 199(1), 18–24 (2009).

25 Fagan AJ, Davies GR, Hutchison JM, Glasser FP, Lurie DJ: Development of a 3-D multi-nuclear continuous wave NMR imaging system. *J. Magn. Reson.* 176(2), 140–150 (2005).

▪ **Good background reading and description of the continuous-wave method.**

26 Navon G, Eliav U, Demco DE, Blümich B: Study of order and dynamic processes in tendon by NMR and MRI. *J. Magn. Reson. Imaging* 25(2), 362–380 (2007).

27 Grenier D, Pascui O, Briguet A: Dipolar contrast for dense tissues imaging. *J. Magn. Reson.* 147, 353–356 (2000).

28 Regatte RR, Schweitzer ME, Jerschow A, Reddy R: Magic sandwich echo relaxation mapping of anisotropic systems. *Magn. Reson. Imaging* 25(3), 433–438 (2007).

29 Haacke EM, Mittal S, Wu Z, Neelavalli J, Cheng YC-N: Susceptibility-weighted imaging: technical aspects and clinical applications, part 1. *AJNR Am. J. Neuroradiol.* 30, 19–30 (2009).

▪ **Good general coverage of susceptibility-weighted imaging.**

30 Mittal S, Wu Z, Neelavalli J, Haacke EM: Susceptibility-weighted imaging: technical aspects and clinical applications, part 2. *AJNR Am. J. Neuroradiol.* 30, 232–252 (2009).

▪ **Good general coverage of susceptibility-weighted imaging.**

31 Du J, Chiang AJ, Chung CB *et al.*: Orientational analysis of the Achilles tendon and enthesis using an ultrashort echo time spectroscopic imaging sequence. *Magn. Reson. Imaging* (2009) (Epub ahead of print).

32 Schäfer A, Wharton S, Gowland P, Bowtell R: Using magnetic field simulation to study susceptibility-related phase contrast in gradient echo MRI. *Neuroimage* 48(1), 126–137 (2009).

33 de Rochefort L, Liu T, Kressler B *et al.*: Quantitative susceptibility map reconstruction from MR phase data using bayesian regularization: validation and application to brain imaging. *Magn. Reson. Med.* 63, 194–206 (2010).

34 Cunningham CH, Arai T, Yang PC, McConnell MV, Pauly JM, Conolly SM: Positive contrast magnetic resonance imaging of cells labeled with magnetic nanoparticles. *Magn. Reson. Med.* 53(5), 999–1005 (2005).

35 Suzuki Y, Cunningham CH, Noguchi K *et al.*: *In vivo* serial evaluation of superparamagnetic iron-oxide labeled stem cells by off-resonance positive contrast. *Magn. Reson. Med.* 60(6), 1269–1275 (2008).

36 Liu W, Frank JA: Detection and quantification of magnetically labeled cells by cellular MRI. *Eur. J. Radiol.* 70(2), 258–264 (2009).

▪ **Coverage of imaging techniques for magnetic iron oxide particles.**

37 Dahnke H, Liu W, Herzka D, Frank JA, Schaeffter T: Susceptibility gradient mapping (SGM): a new postprocessing method for positive contrast generation applied to superparamagnetic iron oxide particle (SPIO)-labeled cells. *Magn. Reson. Med.* 60(3), 595–603 (2008).

38 Liu W, Dahnke H, Rahmer J, Jordan EK, Frank JA: Ultrashort T_2* relaxometry for quantitation of highly concentrated superparamagnetic iron oxide (SPIO) nanoparticle labeled cells. *Magn. Reson. Med.* 61(4), 761–766 (2009).

39 Koch KM, Lorbiecki JE, Hinks RS, King KF: A multispectral three-dimensional acquisition technique for imaging near metal implants. *Magn. Reson. Med.* 61(2), 381–390 (2009).

▪ **Key reference on metal artifact control.**

40 Lu W, Pauly KB, Gold GE, Pauly JM, Hargreaves BA: SEMAC: slice encoding for metal artifact correction in MRI. *Magn. Reson. Med.* 62(1), 66–76 (2009).

▪ **Key reference on metal artifact control.**

41 Cho ZH, Kim DJ, Kim YK: Total inhomogenity correction including chemical shifts and susceptibility by view angle tilting. *Med. Phys.* 15(1), 7–11 (1988).

42 Techawiboonwong A, Song HK, Leonard MB, Wehrli FW: Cortical bone water: *in vivo* quantification with ultrashort echo-time MR imaging. *Radiology* 248(3), 824–833 (2008).

▪ **Clinical application of short T_2 measurements.**

43 Benjamin M, Milz S, Bydder GM: Magnetic resonance imaging of entheses. Part 1. *Clin. Radiol.* 63(6), 691–703 (2008).

44 Benjamin M, Milz S, Bydder GM: Magnetic resonance imaging of entheses. Part 2. *Clin. Radiol.* 63(6), 704–711 (2008).

45 Hauger O, Frank LR, Boutin RD *et al.*: Characterization of the "red zone" of knee meniscus: MR imaging and histologic correlation. *Radiology* 217, 193–200 (2000).

46 Ra JB, Hilal SK, Cho ZH: A method for *in vivo* MR imaging of the short T_2 component of sodium-23. *Magn. Reson. Med.* 3(2), 296–302 (1986).

47 Robson MD, Gatehouse PD, Bydder GM, Neubauer S: Human imaging of phosphorus in cortical and trabecular bone *in vivo*. *Magn. Reson. Med.* 51, 888–892 (2004).

48 Gatehouse PD, He T, Puri BK, Thomas RD, Resnick D, Bydder GM: Contrast-enhanced MRI of the menisci of the knee using ultrashort echo time (UTE) pulse sequences: imaging of the red and white zones. *Br. J. Radiol.* 77, 641–647 (2004).

▪ **Distinction of red and white zones.**

49 Gold GE, Thedens DR, Pauly JM *et al.*: MR imaging of articular cartilage of the knee: new methods using ultrashort TEs. *AJR Am. J. Roentgenol.* 170(5), 1223–1226 (1998).

50 Hall-Craggs MA, Porter J, Gatehouse PD, Bydder GM: Ultrashort echo time (UTE) MRI of the spine in thalassaemia. *Br. J. Radiol.* 77, 104–110 (2004).

51 Waldman A, Rees JH, Brock CS, Robson MD, Gatehouse PD, Bydder GM: MRI of the brain with ultra-short echo-time pulse sequences. *Neuroradiology* 45, 887–892 (2003).

52 Portman O, Flemming S, Cox JP, Johnston DG, Bydder GM: Magnetic resonance imaging of the normal pituitary gland using ultrashort TE (UTE) pulse sequences. *Neuroradiology* 50, 213–220 (2008).

53 Chappell KE, Patel N, Gatehouse PD *et al*: Magnetic resonance imaging of the liver with ultrashort TE (UTE) pulse sequences. J. *Magn. Reson. Imaging* 18, 709–713 (2003).

54 Wansapura JP, Daniel BL, Vigen KK, Butts K: *In vivo* MR thermometry of frozen tissue using R_2* and signal intensity. *Acad. Radiol.* 12, 1080–1084 (2005).

55 Filho GH, Du J, Pak BC *et al*: Quantitative characterization of the Achilles tendon in cadaveric specimens: T_1 and T_2* measurements using ultrashort-TE MRI at 3T. *AJR Am. J. Roentgenol.* 192, 117–124 (2009).

56 Du J, Pak BC, Znamirowski R *et al.*: Magic angle effect in magnetic resonance imaging of the Achilles tendon and enthesis. *Magn. Reson. Imaging* 27, 557–564 (2009).

57 Gurney PT, Hargreaves BA, Nishimura DG: Design and analysis of a practical 3D cones trajectory. *Magn. Reson. Med.* 55, 575–582 (2006).

58 Du J, Takahashi AM, Bydder M, Chung CB, Bydder GM: Ultrashort TE imaging with off-resonance saturation contrast (UTE-OSC). *Magn. Reson. Med.* 62, 527–531 (2009).

59 Springer F, Martirosian P, Machann J, Schwenzeer NF, Claussen CD, Schick F: Magnetization transfer contrast imaging in bovine and human cortical bone applying an ultrashort echo time sequence at 3 Tesla. *Magn. Reson. Med.* 61, 1040–1048 (2009).

60 Robson MD, Gatehouse PD, So PW, Bell JD, Bydder GM: Contrast enhancement of short T_2 tissues using ultrashort TE (UTE) pulse sequences. *Clin. Radiol.* 59, 720–726 (2004).

61 Crowe LA, Wang Y-X, Gatehouse P *et al.*: *Ex vivo* MR imaging of atherosclerotic rabbit aorta labeled with USPIO – enhancement of iron loaded regions in UTE imaging. *Proc. Intl Soc. Mag. Reson. Med.* 13, 115 (2005).

62 O'Brien KR, Myerson SG, Cowan BR, Young AA, Robson MD: Phase contrast ultrashort TE: a more reliable technique for measurement of high-velocity turbulent stenotic jets. *Magn. Reson. Med.* 62, 626–636 (2009).